Supporting Information

Rational design of nanoporous Cu-Co-Ni-P nanotube arrays and $CoFe_2Se_4$ nanosheet arrays for flexible solid-state asymmetric devices

Akbar Mohammadi Zardkhoshoui* and Saied Saeed Hosseiny Davarani*

Department of Chemistry, Shahid Beheshti University, G. C., 1983963113, Evin, Tehran, Iran.

Corresponding authors: *Tel: +98 21 22431661; Fax: +98 21 22431661; E-mail: ss-hosseiny@sbu.ac.ir (S.S.H. Davarani); and mohammadi.bahadoran@gmail.com (A. Mohammadi Zardkhoshoui)

Preparation of the PVA/KOH gel electrolyte

The PVA/KOH gel electrolyte was prepared using mixing 500 mg poly (vinyl alcohol) (PVA) powder with 500 mg KOH in 5ml DI water and mixed at 60˚ for 60 min, while continuously stirring until it took on a clear appearance and homogeneous viscous.

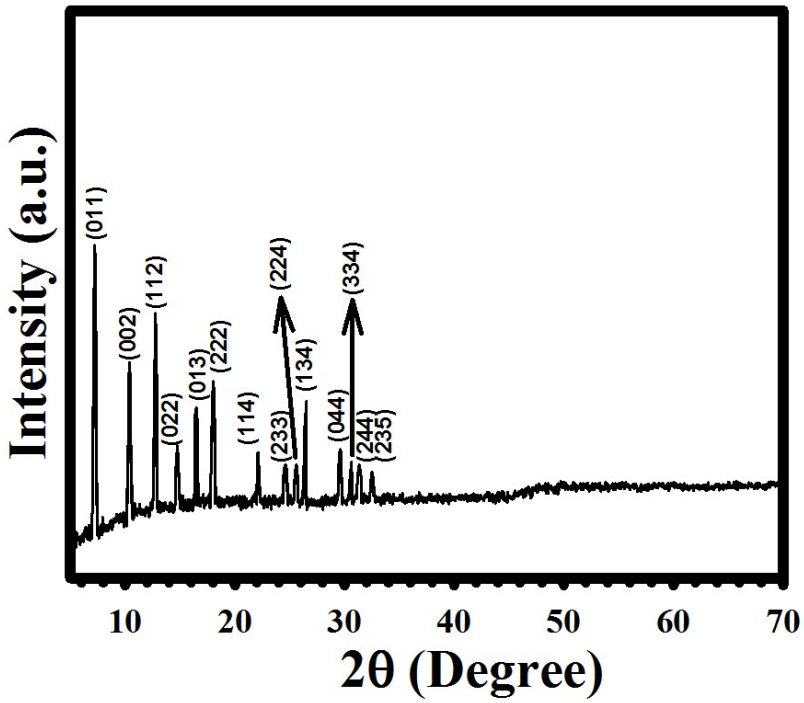

Fig. S1. XRD pattern of the Cu-Co-Ni MOF precursor.

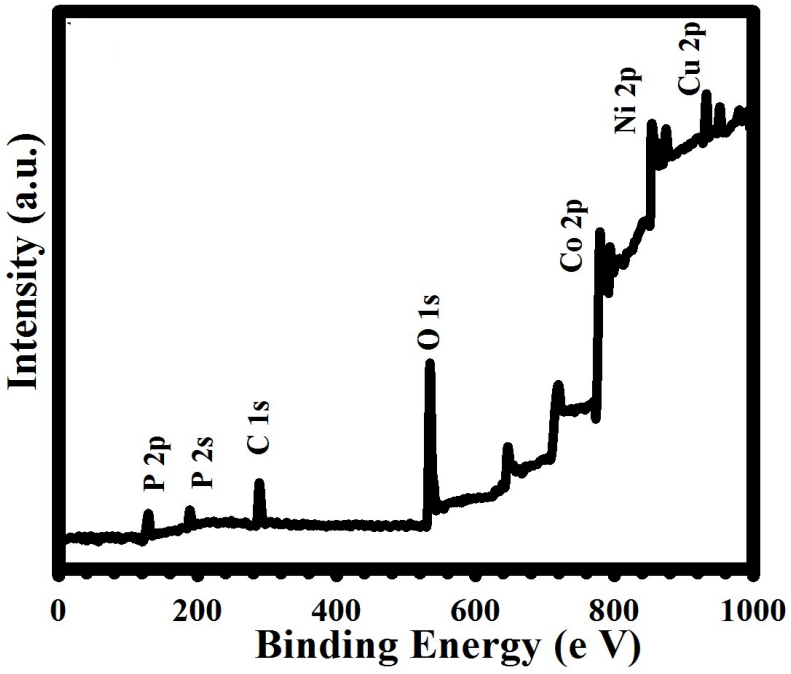

Fig. S2. Survey spectrum of the CCNP-NA sample.

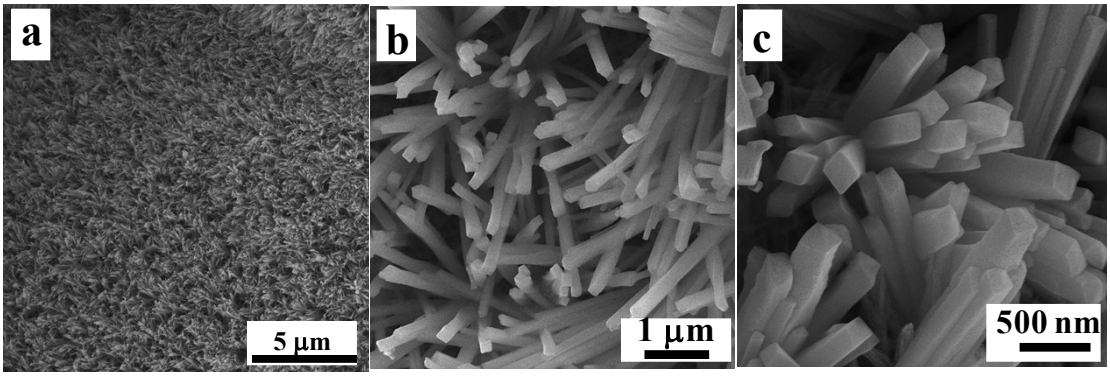

Fig. S3. (a-c) FE-SEM images of the Cu-Co-Ni-MOF precursor.

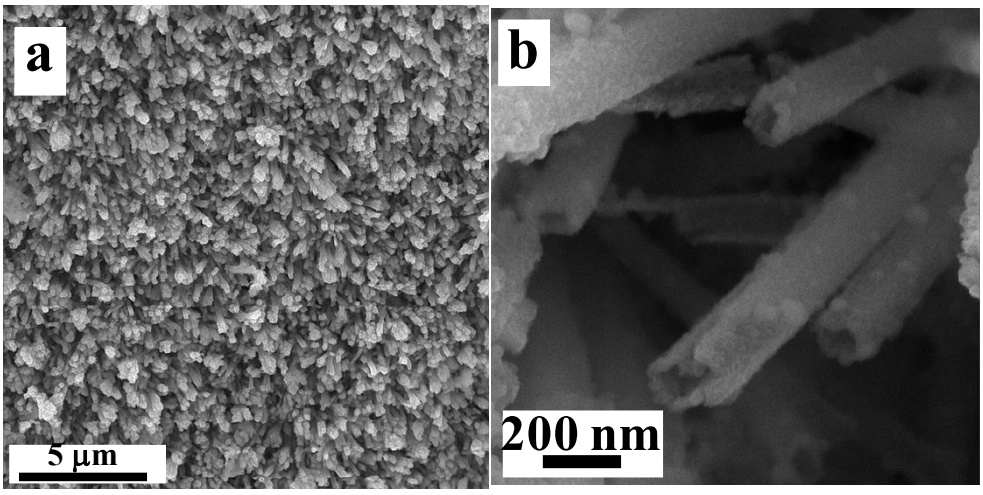

Fig. S4. (a, b) FE-SEM images of the Cu-Co-Ni-oxide.

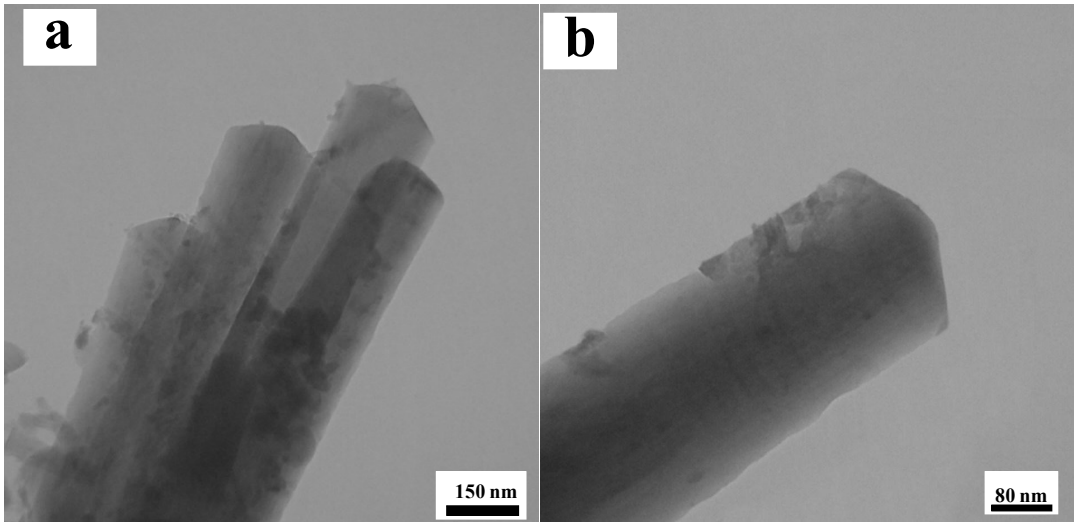

Fig. S5. (a, b) TEM images of the Cu-Co-Ni-MOF precursor.

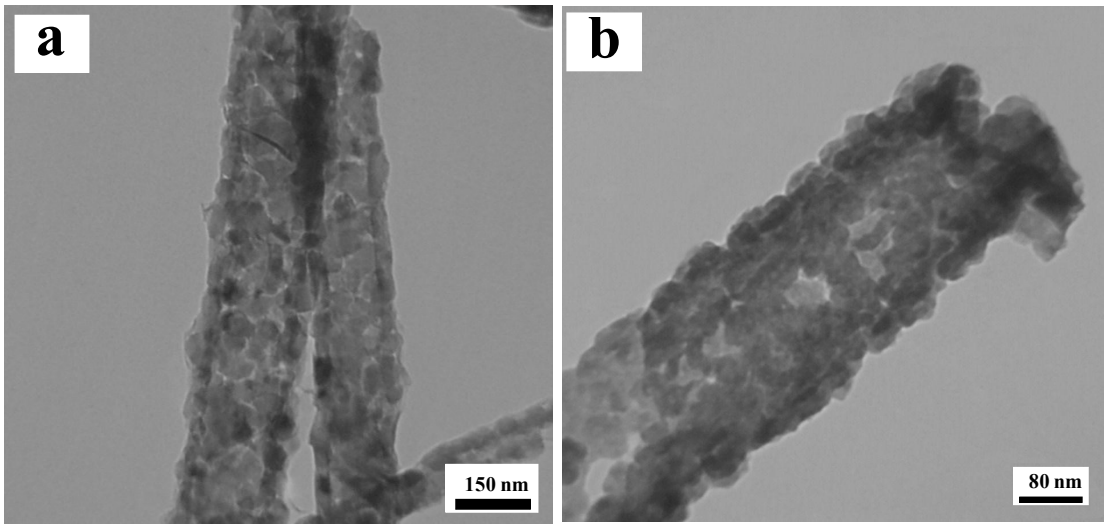

Fig. S6. (a, b) TEM images of the Cu-Co-Ni-oxide.

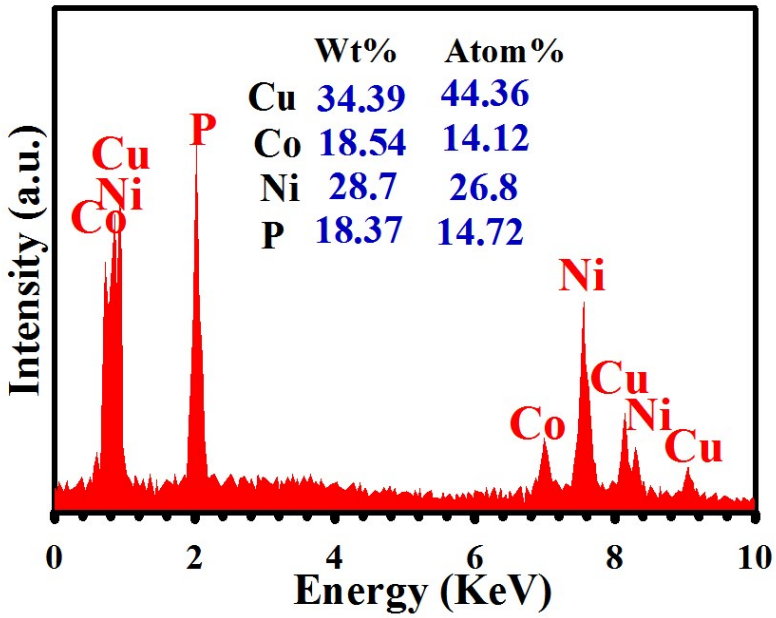

Fig. S7. EDAX analysis of CCNP-NA.

Based on the weight of Cu (34.39 wt%) and P (18.37 wt%) elements, the content of Cu_3P in the CuCoNi-P is calculated as about 40.51 wt% (34.39 wt% + 18.37/3 wt%), the content of CoP in the CuCoNi-P is calculated as about 24.66 wt% (18.54 wt% + 18.37/3 wt%), and the content of Ni_2P in the CuCoNi-P is calculated as about 34.83 wt% (28.7 wt% + 18.37/3 wt%).

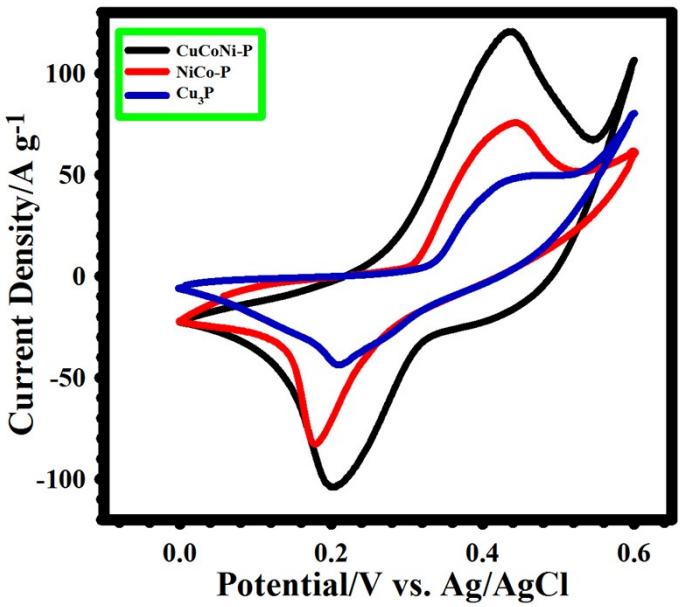

Fig. S8. CV curves of Cu_3P, NiCo-P and CuCoNi-P electrodes at scan rate of 30 mV s^{-1}.

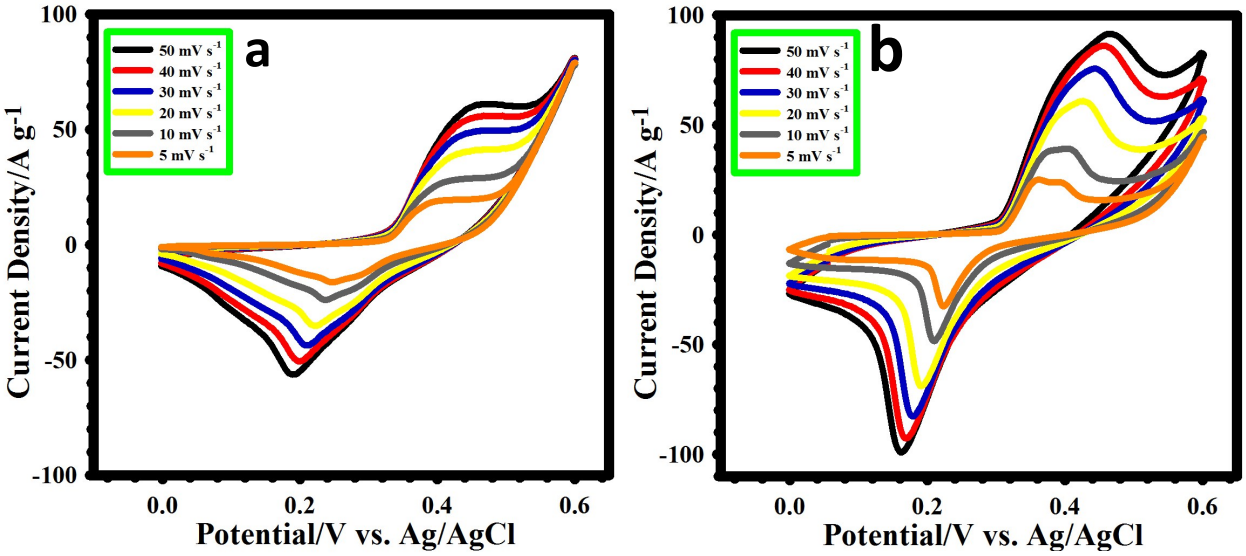

Fig. S9. (a) CV curves of the Cu_3P electrode at various scan rates. (b) CV curves of the NiCo-P electrode various scan rates

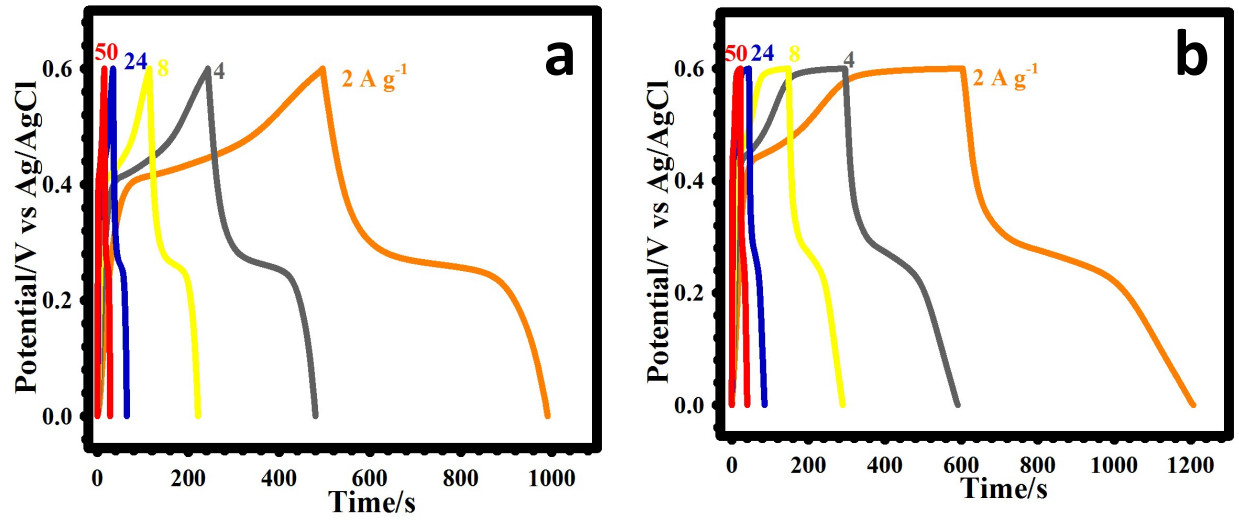

Fig. S10. (a) GCD plots of the Cu_3P electrode at various current densities. (b) GCD plots of the NiCo-P electrode at various current densities

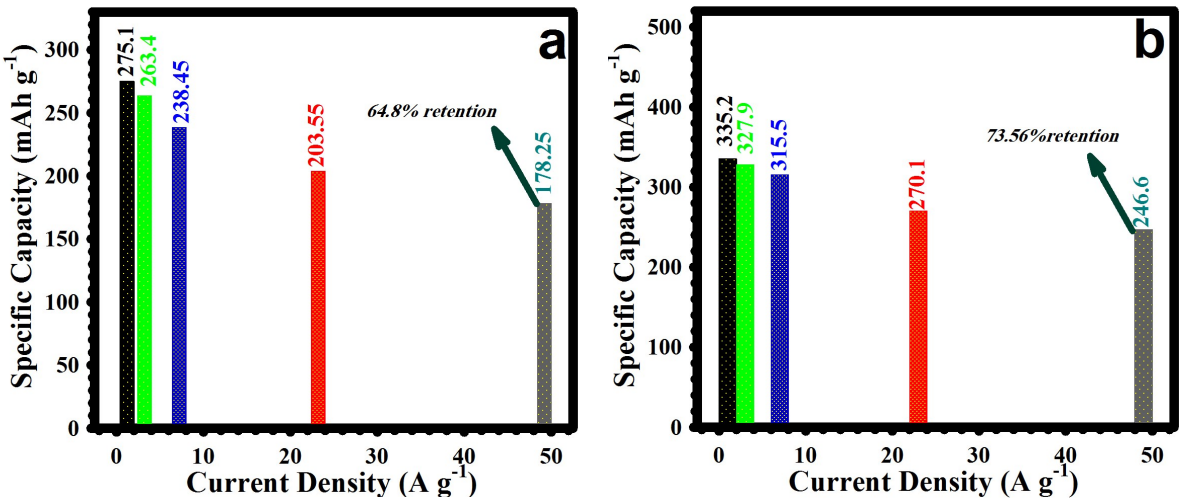

Fig. S11. (a) Rate capability of the Cu_3P electrode. (b) Rate capability of the NiCo-P electrode.

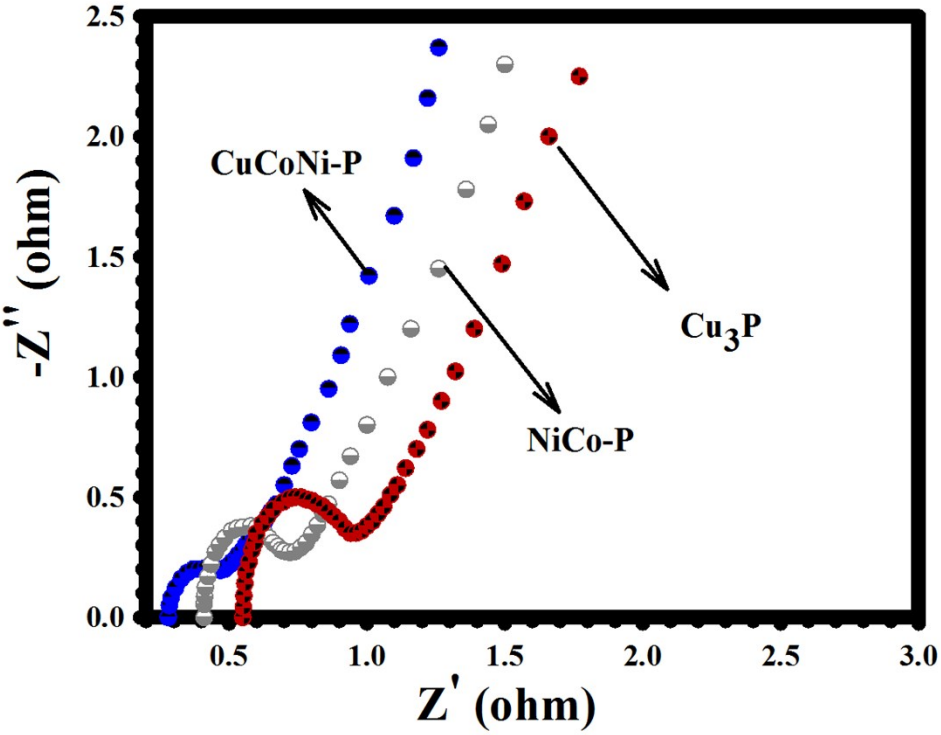

Fig. S12. Nyquist graph of the Cu_3P, NiCoP, and CuCoNi-P electrodes.

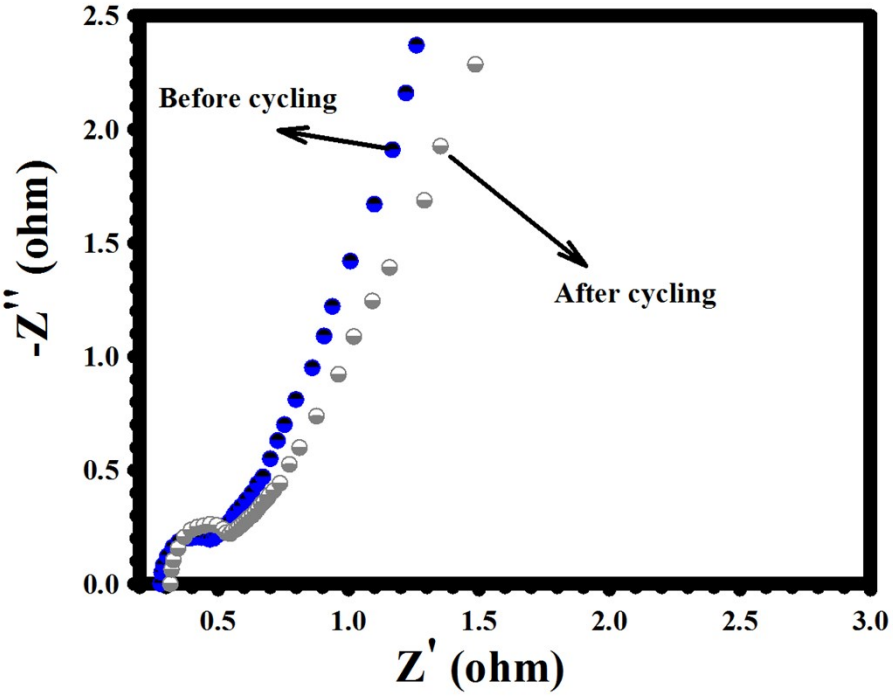

Fig. S13. Nyquist graph of the CuCoNi-P electrode before and after cycling.

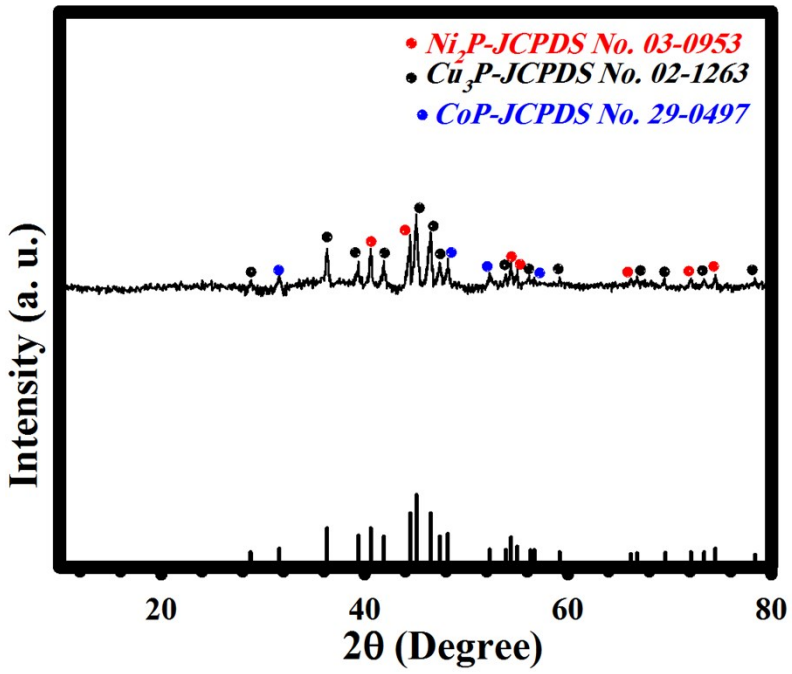

Fig. S14. XRD pattern of the Cu-Co-Ni-P after cycling test

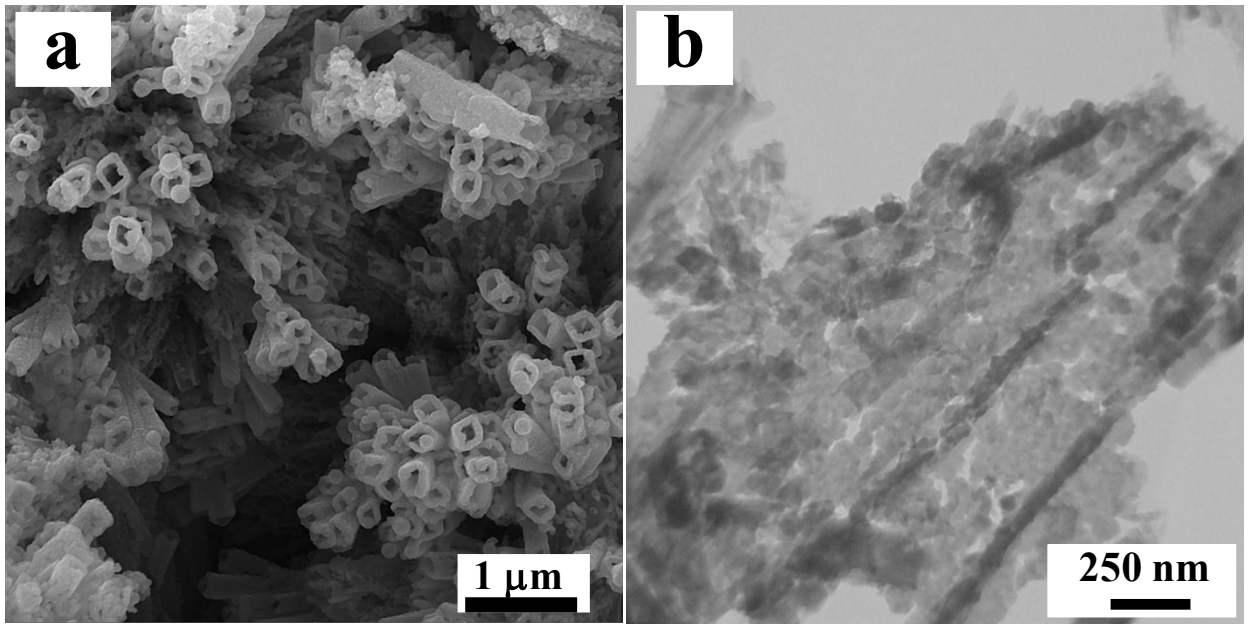

Fig. S15. (a and b) FE-SEM and TEM images of the Cu-Co-Ni-P after cycling test.

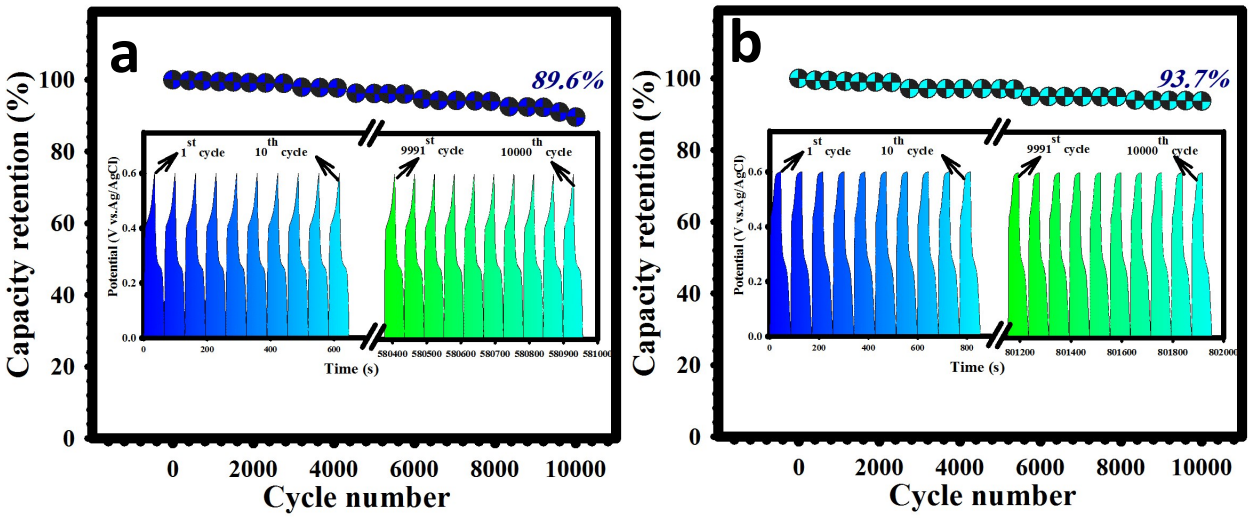

Fig. S16. (a) Durability test of the Cu_3P electrode. (b) Durability test of the NiCo-P electrode.

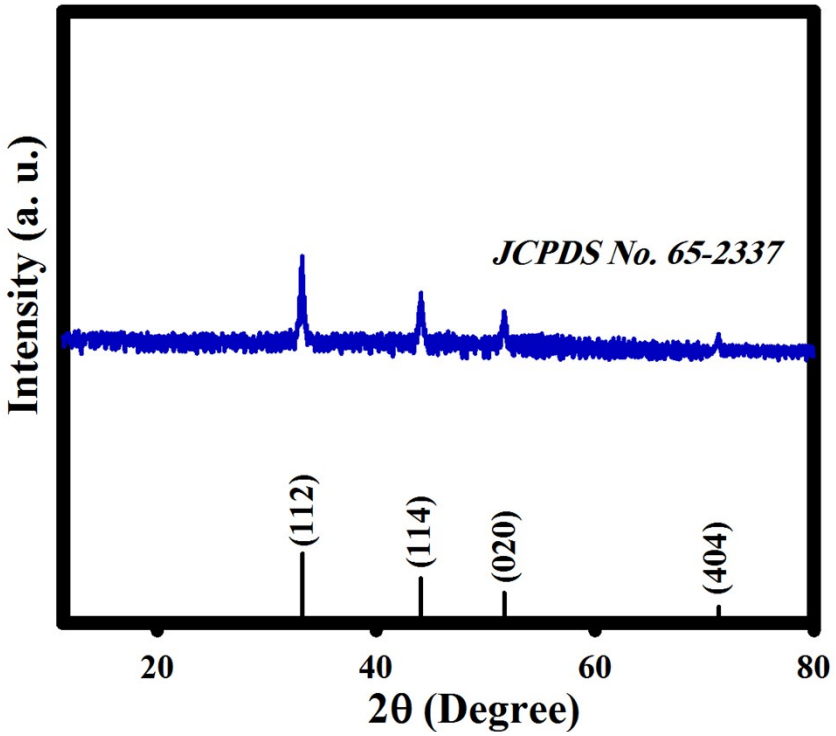

Fig. S17. XRD pattern of the CFS-NA after cycling test.

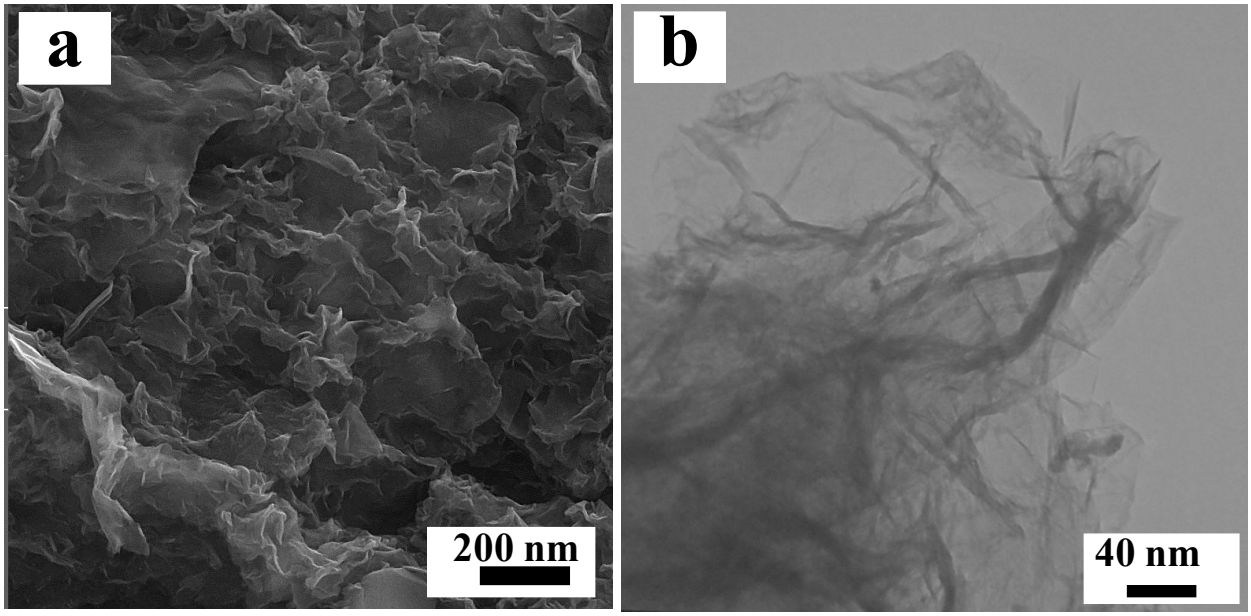

Fig. S18. (a and b) FE-SEM and TEM images of the CFS-NA after cycling test.

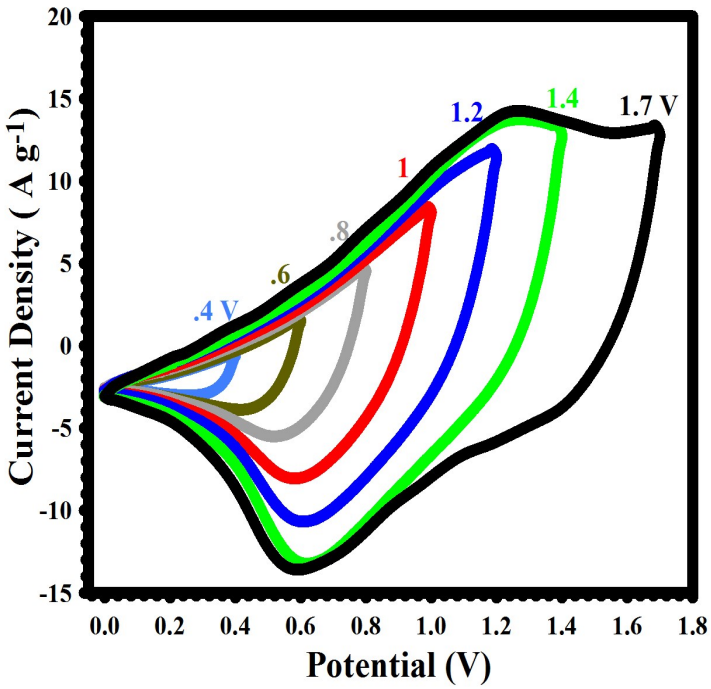

Fig. S19. CV curves of the device at various potential windows.

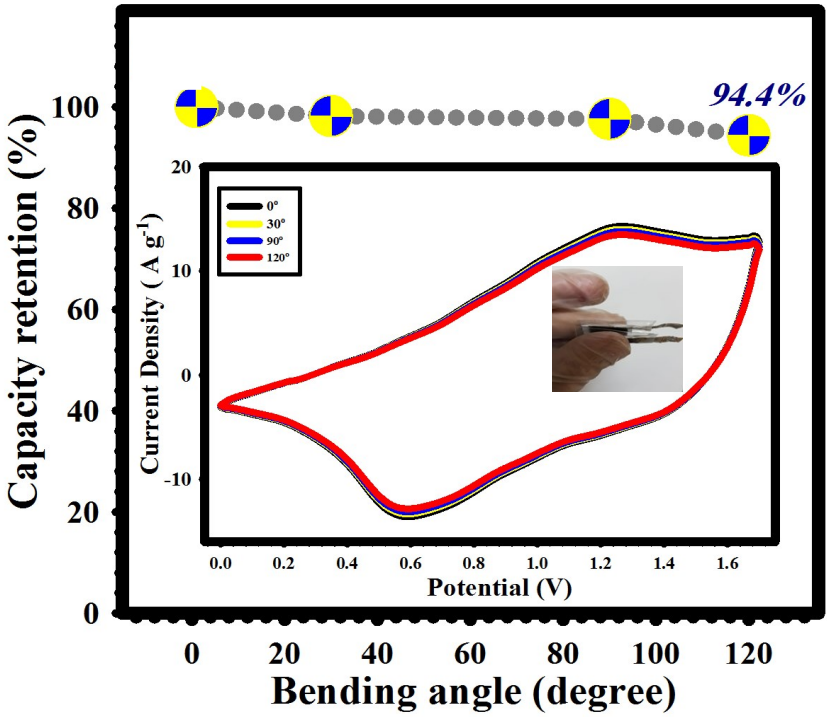

Fig. S20. CV plots of the device with various bending angles.

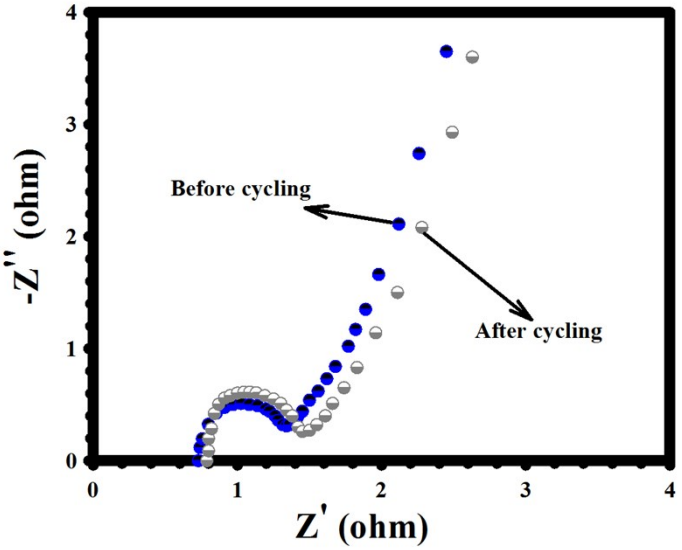

Fig. S21. Nyquist graphs of the device before and after cycling test.

Table S1. Comparison of the electrochemical performance of positive electrode in three and two electrode systems with other previously reported electrodes

Composition	*Capacity 3 and 2 electrodes (mAh g^{-1})*	Cycles, retention 2 and 3 electrode	ED (W h kg^{-1}) 2 Electrode	Reference
NiMn-1	*385.6 at .68 A g^{-1} (3 E)* *59.7* at .47 A g^{-1} *(2 E)*	*3000, 95.6% (3 E)* *5000, 85.3% (2 E)*	51.5	1
$NiCo_2S_4$	*301.1 at 2 A g^{-1} (3 E)* *80.56* at 1 A g^{-1} *(2 E)*	*5000, 93.85% (2 E)*	*48.65*	2
$MnCo_2O_{4.5}$@$Ni(OH)_2$	*318 at 3 A g^{-1} (3 E)* *70.67 at 1 A g^{-1} (2 E)*	*5000, 87.7% (3 E* *3000, 90.4% (2 E)*	*56.53*	3
Ni-MOF	*123.5 at 1 A g^{-1} (3 E)*	*3000, 90.6% (2 E)*	*55.8*	4
Co_3O_4	*209 at 1 A g^{-1} (3 E)*	*3000, 90 (3 E)*	41.4	5
$NiCo_2O_4$	*130 at .63 A g^{-1} (3 E)*	*100, 100 (3 E)*	*16.6*	6
NiO	119.7 at 2 A g^{-1} (3 E) 28.3 at 2 A g^{-1} (2 E)	5000, 84.2% (3 E) 5000, 85.2% (2 E)	48	7
Co-Cd-Se	192 (3 E) at 1 A g^{-1} 85 (2 E) at 1 A g^{-1}	1000, 95.2% (3 E) 1000, 80.9% (2 E)	57.6	8
$ZnCo_2O_4$	78.89 at 1 A g^{-1} (3 E) 34.7 at .2 A g^{-1} (2 E)		27.78	9
Co_3O_4/$Co(OH)_2$	184.9 at 1 A g^{-1} (3 E) 58.9 4 A g^{-1} (2 E)	5000, 90% (3 E) 5000, 91% (2 E)	37.6	10
$NiCo_2S_4$@$Ni(OH)_2$	404.2 at 2 A g^{-1} (3 E)	5000, 90% (3 E) 6000, 97% (2 E)	83	11

CCNP-NA	**406.73 (3 E)** **180.6 (2 E)**	**10000, 98.9 (3 E)** **10000, 96.2% (2 E)**	**153.5**	**This work**

References:

1. L. Ye, Y. T. Zhou, Z. Bao, Y. Zhao, Y. Zou, L. Zhao and Q. Jiang, Sheet-membrane Mn-doped nickel hydroxide encapsulated via heterogeneous Ni_3S_2 nanoparticles for efficient alkaline battery–supercapacitor hybrid device, *J. Mater. Chem. A* 2018, **6**, 19020-19029.

2. K. Zheng, G. Li and C. Xu, Advanced battery-supercapacitor hybrid device based on Co/Ni-ZIFs-derived $NiCo_2S_4$ ultrathin nanosheets electrode with high performance, *Appl. Surf. Sci.* 2019, **490**, 137-144.

3. Y.-L. Liu, C. Yan, G.-G. Wang, H.-Y. Zhang, L.-Y. Dang, B.-W. Wu, Z.-Q. Lin, X.-S. An and J. Han, Achieving Ultrahigh Capacity with Self-Assembled $Ni(OH)_2$ Nanosheet-Decorated Hierarchical Flower-like $MnCo_2O_{4.5}$ Nanoneedles as Advanced Electrodes of Battery–Supercapacitor Hybrid Devices, *ACS Appl. Mater. Interfaces* 2019, **11**, 9984-9993.

4. Y. Jiao, J. Pei, C. Yan, D. Chen, Y. Hu and G. Chen, Layered nickel metal–organic framework for high performance alkaline battery-supercapacitor hybrid device, *J. Mater. Chem. A* 2016, **4**, 13344-13351

5. L. Zhang, Y. Zhang, S. Huang, Y. Yuan, H. Li, Z. Jin, J. Wu, Q. Liao, L. Hu, J. Lu, S. Ruan and Y.-J. Zeng, Co_3O_4/Ni-based MOFs on carbon cloth for flexible alkaline battery-supercapacitor hybrid devices and near-infrared photocatalytic hydrogen evolution, *Electrochim. Acta* 2018, **281**, 189-197.

6. Y. Yuan, Y. Lu, B.‐E. Jia, H. Tang, L. Chen, Y.‐J. Zeng, Y. Hou, Q. Zhang, Q. He, J. Leng, Z. Ye and J. Lu, Integrated System of solar Cells with Hierarchical $NiCo_2O_4$ Battery-

Supercapacitor Hybrid Devices for Self-driving Light-emitting Diodes, *Nano-Micro Lett*. 2019, **42**, 2-12.

7. J. Lin, Y. Yan, H. Wang, X. Zheng, Z. Jiang, Y. Wang, J. Qi, J. Cao, W. Fei and J. Feng, Hierarchical Fe_2O_3 and NiO nanotube arrays as advanced anode and cathode electrodes for high-performance asymmetric supercapacitors, *J. Alloys Compd*. 2019, **794**, 255-260.

8. Z.-B. Zhai, K.-J. Huang and X. Wu, Superior mixed Co-Cd selenide nanorods for high performance alkaline battery-supercapacitor hybrid energy storage, *Nano Energy* 2018, **47**, 89-95.

9. Y. Shang, T. Xie, C. Ma, L. Su, Y. Gai, J. Liu and L. Gong, Synthesis of hollow $ZnCo_2O_4$ microspheres with enhanced electrochemical performance for asymmetric supercapacitor, *Electrochim. Acta* 2018, **286**, 103-113.

10. G. Lee and J. Jang, High-performance hybrid supercapacitors based on novel $Co_3O_4/Co(OH)_2$ hybrids synthesized with various-sized metal-organic framework templates, *J. Power Sources* 2019, **423**, 115-124.

11. B. Shi, B. Saravanakumare, W. Wei, G. D. S. Wu, X. Lu, M. Zeng, X. Gao, Q. Wang, G. Zhou, J.-M. Liu, K. Kempa and J. Gao, 3D honeycomb $NiCo_2S_4@Ni(OH)_2$ nanosheets for flexible all-solid-state asymmetric supercapacitors with enhanced specific capacitance, *J. Alloys Compd*. 2019, **790**, 693-702.

.